In vitro magnetosome remineralization for silver-magnetite hybrid magnetosome biosynthesis and used for healing of the infected wound

Junjie Xu[1,2†], Shijiao Ma[2†], Wei Zhang[1], Lina Jia[1], Haolan Zheng[2], Pang Bo[2], Xue Bai[1], Hongyan Sun[1], Lei Qi[3], Tongwei Zhang[4], Chuanfang Chen[5], Feng Li[6], Fumihito Arai[7], Jiesheng Tian[2*] and Lin Feng[1*]

Abstract

Background: Magnetosomes (BMPs) are organelles of magnetotactic bacteria (MTB) that are responsible for mineralizing iron to form magnetite. In addition, BMP is an ideal biomaterial that is widely used in bio- and nano-technological applications, such as drug delivery, tumor detection and therapy, and immunodetection. The use of BMPs to create multifunctional nanocomposites would further expand the range of their applications.

Results: In this study, we firstly demonstrate that the extracted BMP can remineralize in vitro when it is exposed to $AgNO_3$ solution, the silver ions (Ag^+) were transported into the BMP biomembrane (MM) and mineralized into a silver crystal on one crystal plane of Fe_3O_4. Resulting in the rapid synthesis of an Ag-Fe_3O_4 hybrid BMP (BMP-Ag). The synergy between the biomembrane, Fe_3O_4 crystal, and unmineralized iron enabled the remineralization of BMPs at an Ag^+ concentration $\geq$ 1.0 mg mL^{-1}. The BMP-Ag displayed good biocompatibility and antibacterial activity. At a concentration of 2.0 mg/mL, the BMP-Ag and biomembrane removed Ag-Fe_3O_4 NPs inhibited the growth of gram-negative and gram-positive bacteria. Thus using BMP-Ag as a wound dressing can effectively enhance the contraction of infected wounds.

Conclusions: This study represents the first successful attempt to remineralize organelles ex vivo, realizing the biosynthesis of hybrid BMP and providing an important advancement in the synthesis technology of multifunctional biological nanocomposites.

Keywords: Biomaterial, Nanocomposites, Remineralization, Ag-Fe_3O_4 hybrid magnetosome, Biosynthesis

---

[†]Junjie Xu and Shijiao Ma contributed equally to this work

*Correspondence: tianhome@cau.edu.cn; linfeng@buaa.edu.cn

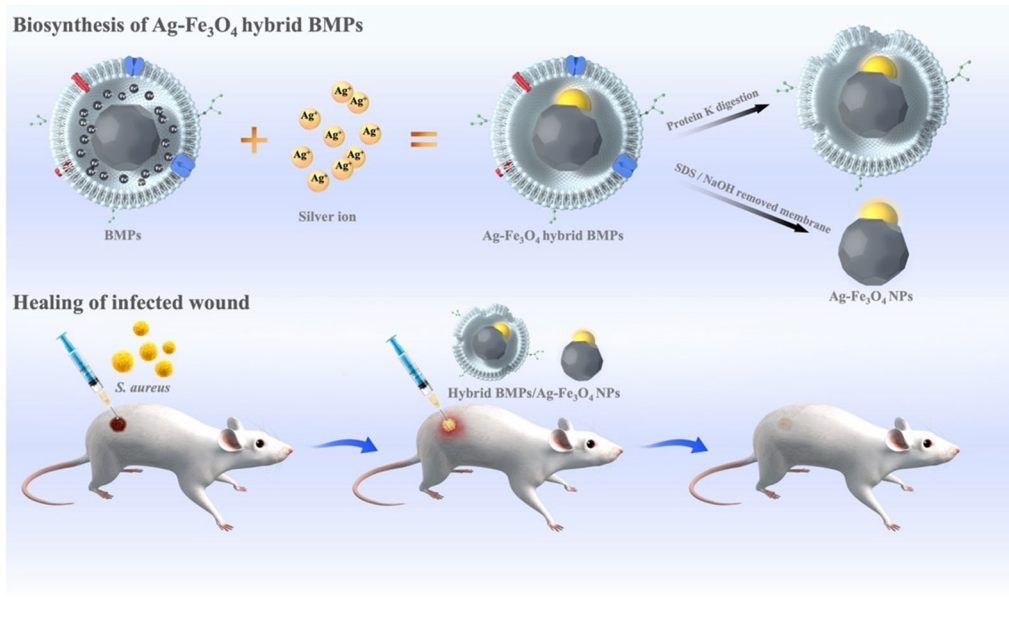[1] School of Mechanical Engineering and Automation, Beihang University, Beijing 100083, China
[2] State Key Laboratory of Agrobiotechnology, College of Biological Sciences, China Agricultural University, Beijing 100193, China
Full list of author information is available at the end of the article

Xu *et al. Journal of Nanobiotechnology*   (2022) 20:364

Page 2 of 14

Graphical abstract

Biosynthesis of Ag-Fe$_3$O$_4$ hybrid BMPs

BMPs + Silver ion = Ag-Fe$_3$O$_4$ hybrid BMPs

Protein K digestion

SDS / NaOH removed membrane

Ag-Fe$_3$O$_4$ NPs

Healing of infected wound

S. aureus → Hybrid BMPs/Ag-Fe$_3$O$_4$ NPs →

Background

Biomineralization provides specialized biological functions for living organisms, such as mechanical support (e.g., in bones), protection (e.g., in molluscan shells), and mineral storage (e.g., in magnetotactic bacteria magnetosomes). Furthermore, biomineralization plays an important role in biogeochemical element cycles [1]. MTB can absorb iron from the environment and mineralize it to form magnetite nanoparticles (NPs) in its organelle BMPs, contributing significantly to the iron cycle and presenting an elegant example of prokaryote biomineralization [2, 3]. Recently various biological functions of BMPs have been reported, including magnetic navigation [4, 5], iron- and energy-storing abilities [6–8], and the decreased accumulation of free radicals in cells as well as their elimination [9, 10].

In addition, MTB and BMP are ideal candidates for application as microrobots and bionanomaterials, which are widely used in drug delivery, tumor detection and therapy, and immunodetection [11–17], but single-component nanomaterials do not meet the requirements for certain fields. A variety of multifunctional composites have already been synthesized [18–20], primarily based on chemical methods. However, many reagents used during the manufacturing have severely adverse environmental effects and eventually harm human health [21].

Currently, nanoparticles synthesis relates to simple, cost-effective, and eco-friendly methods with multifunctional properties [22, 23]. Green synthesis of nanomaterials includes synthesis at mild pH, pressure, and temperature. It does not entail hazardous substances and avoids addition of external reducing, capping, and stabilizing agents [24, 25]. Green synthesis also facilitate the application of nanomaterials [known as nanobiotechnology] as these nanoproducts are generally biocompatible [25]. A promising method is to biosynthesize nanocomposite via MTB. MTB can synthesize Co, Mn, and Cu-doped BMP in vivo [26–29], which exhibits better magnetic hyperthermia than BMP [30].

Among nanocomposites, two or more functional nanoparticles formed nanohybrids often reveal much better performance in some properties or even generate new features due to the interfacial effect and coupling effect [31–33]. Nevertheless, the biosynthesis of nanohybrids is a challenging. To the best of our knowledge, there have been few reports on nanohybrids biosynthesis [34] and none on asymmetric hybrid metallic nanoparticles by biosynthesis. The situation greatly hinders the application of nanomaterial green synthesis. Therefore, we developed a simple method to biosynthesize asymmetric nanoparticles, via an efficient way of remineralization of ex vivo BMP. We first found that BMP possessing in vitro bioactivity, can transport Ag$^+$ into the BMP membrane and mineralized into Ag NPs grown on the magnetite crystal surface, forming an Ag-Fe$_3$O$_4$ hybrid BMP.

Unsuccessful wound healing caused by bacterial infection is a severe health problem, leading to millions of deaths every year [35]. The bacteria *P. aeruginosa* easily generate biofilm, *E. coli* is representative of gram-negative bacteria, and *S. aureus* is representative of

Xu *et al. Journal of Nanobiotechnology*   (2022) 20:364

Page 3 of 14

gram-positive bacteria, which can cause several serious infections [36]. Conventional antibiotic has greatly protected the public from bacterial infection, but the large doses of abuse largely increase the drug resistance of bacteria [37]. To solve this problem, engineered materials have been developed to efficiently treat bacterial infections [38–40]. Silver and Fe_3O_4 nanoparticles have attracted researchers' interest in medical devices [41, 42]. Silver nanoparticles (AgNPs) have been widely used in wound healing because of their antimicrobial properties and inhibition of inflammation [43]. Noble-metal-magnetic heterostructures displayed low biotoxicity by preventing the Ag^+ release rate from the cathodic Ag. Therefore, we further explored the potential of the hybrid BMP to treat bacterial infections efficiently.

Results and discussion

BMP production and purification

BMPs are magnetite nanoparticles synthesized by magnetotactic bacteria that can be achieved through cell disruption and magnetic separation [44, 45]. The preparation process of BMP is shown in (Fig. 1A). Firstly, the magnetotactic bacteria were cultured in a fermenter; then, the cell was collected and disrupted by ultrasonication, and the magnet separated the BMP. Compared with other magnetotactic bacteria, *M. gryphiswaldense* MSR-1 is more suitable for fermenter cultivation. The cell and BMP yield was 2–threefold higher than those of *Magnetospirillum magneticum* AMB-1 and *Magnetospirillum magnetotacticum* MS-1 [32].

A fed-batch culture of MSR-1 was conducted in a 42-L fermenter for production of BMP. Cell density (OD_{565}) and magnetic response (Cmag value) were detected in the culture process. After 44 h of culture, OD_{565} and Cmag reached approximately 10.5 and 1.2, respectively (Fig. 1B). Owing to the Cmag value decreasing continuously, MSR-1 fermenter cultivation terminated. The total cell collected was approximately 102.7 g, and the working volume of the fermenter was 30 L; therefore, the cell yield was approximately 3.42 g L^{-1}. In fermenter-cultured MSR-1, TEM observation showed that BMPs were arranged in a chain along the cell (Fig. 1C, black arrow).

BMP was purified from the collected cell following several rounds of ultrasonication and magnetic capturing (Fig. 1D, black arrow). The total BMP gained was approximately 6.65 g, and the magnetosome yield was approximately 221.7 mg L^{-1}. TEM observation showed that the purified BMP was pure, and there were no protein fragments on BMPs and background (Fig. 1E). BMP was washed 3–5 times in deionized water using an ultrasonic cleaner to remove the remaining PO_4^{3-} and Cl^- from the lysis buffer; then, it was used for Ag^+ mineralization.
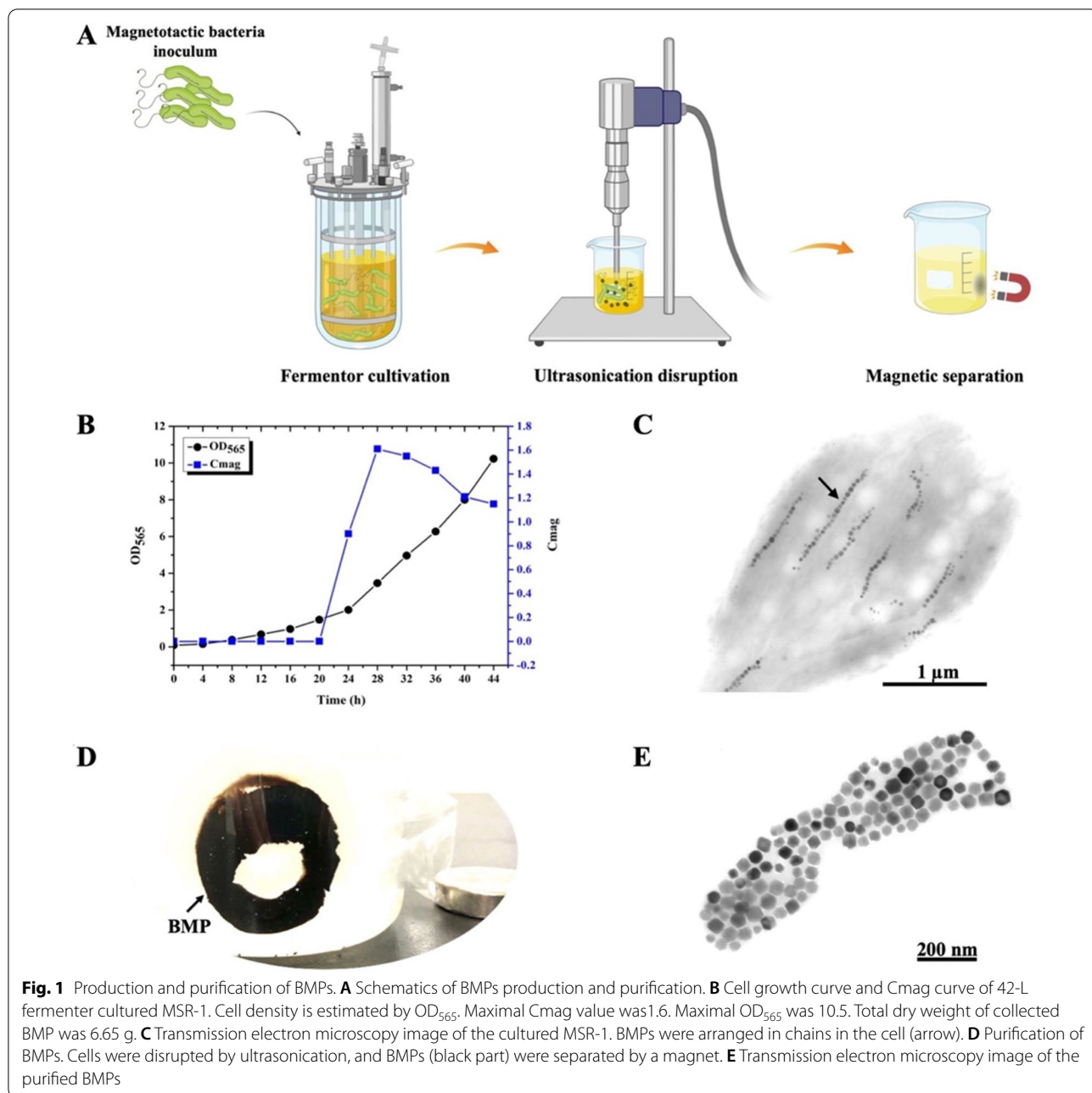
BMP in vitro remineralization and characterization

The purified BMP was incubated with $AgNO_3$ solution. BMP possessed in vitro bioactivity; it transported Ag^+ into the BMP membrane and was remineralized into a Ag-Fe_3O_4 hybrid BMP (Fig. 2A, B). The lattices of Ag and Fe_3O_4 were staggered at the interface (Fig. 2C read arrow), which allowed electron transfer in each component and effectively modulated the physical and chemical properties of the BMP. When the outer biomembrane of the hybrid BMP was removed, the Ag NPs did not separate from the Fe_3O_4 crystals (Fig. 2D). In Co-, Mn-, and Cu-doped BMP, metal elements are always positioned near the surface of BMP, rather than in the core, and these cannot form crystals [24]. In this study, Ag^+ was successfully mineralized into Ag crystals on the plane of Fe_3O_4 crystals, thereby realizing the in vitro biosynthesis of multifunctional heterogeneous hybrid BMPs.

The elemental composition of the hybrid BMP was further confirmed by high-angle annular dark-field scanning transmission electron microscopy (HAADF-STEM), energy-dispersive spectroscopy (EDS), and X-ray photoelectron spectroscopy (XPS). HAADF-STEM Ag and Fe elemental mapping indicated that the NPs synthesized on the Fe_3O_4 crystal plane were Ag NPs (Fig. 2E). EDS analysis of the Ag NPs of the hybrid BMP also demonstrated that excluding most Cu elements from the sample rod, followed by Ag elements, at ~18.5% (Fig. 2F). XPS results showed that compared with BMP, Ag-Fe_3O_4 hybrid BMP exhibited characteristic Ag diffraction peaks (Fig. 2G). The statistical diameter distributions of the Ag NPs of the hybrid BMP are shown in Fig. 2H. The distribution of Ag NPs was narrow and ranged from 5 to 16 nm and mainly concentrated at 9–10 nm; the average diameter was ~10 nm (Fig. 2H). Throughout the remineralization process of BMP, except for the $AgNO_3$ solution, no other elements were added. Therefore, the synthesized NPs on the Fe_3O_4 crystal were most likely Ag NPs, as confirmed by the HAADF-STEM, XPS, and EDS results.

BMP remineralization conditions

Biomineralization always occurs under particular physical and chemical conditions. The factors that affect BMP remineralization were evaluated by changing the $AgNO_3$ concentration, incubation time, and temperature. Freshly extracted BMP was washed 3–5 times in deionized water using an ultrasonic cleaner to remove the remaining PO_4^{3-} and Cl^- from the lysis buffer and then incubated with $AgNO_3$ solution under different conditions.

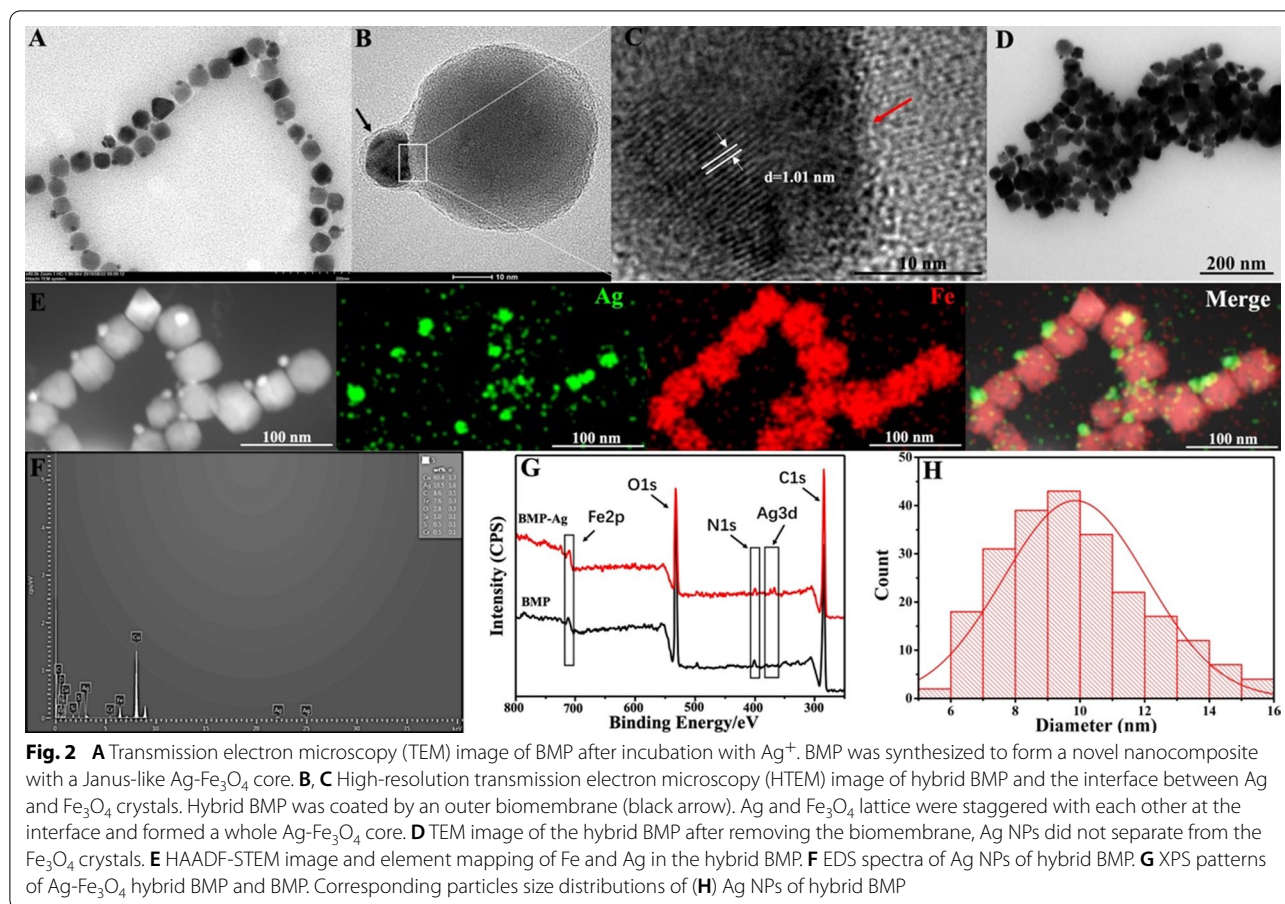A small amount of BMP could mineralize into the Ag-Fe_3O_4 hybrid BMP at a $AgNO_3$ concentration of 0.1 mg mL^{-1} (Fig. 3A, black arrow). When the concentration increased to 1.0 mg mL^{-1}, all BMPs were

Xu *et al. Journal of Nanobiotechnology*   (2022) 20:364

Page 4 of 14

Fig. 1 Production and purification of BMPs. **A** Schematics of BMPs production and purification. **B** Cell growth curve and Cmag curve of 42-L fermenter cultured MSR-1. Cell density is estimated by OD_{565}. Maximal Cmag value was1.6. Maximal OD_{565} was 10.5. Total dry weight of collected BMP was 6.65 g. **C** Transmission electron microscopy image of the cultured MSR-1. BMPs were arranged in chains in the cell (arrow). **D** Purification of BMPs. Cells were disrupted by ultrasonication, and BMPs (black part) were separated by a magnet. **E** Transmission electron microscopy image of the purified BMPs

remineralized (Fig. 3A). The mineralization process of freshly purified BMP completed rapidly within 1 min, at an $AgNO_3$ concentration above 1.0 mg mL^{-1}(Fig. 3B). The diameter of the synthesized Ag NPs did not significantly increase with the increasing incubation time. As the BMP storage time increased, the incubation time also increased, and nearly all types of BMP were able to eradicate remineralization within 30 min. BMP was able to remineralize at different temperatures, and the diameter of the synthesized Ag NPs did not significantly increase from 4 to 40 °C (Fig. 3C). When the temperature was increased to 80 °C, the diameter of the Ag NPs increased by approximately two folds (Additional file 1: Fig. S1). The crystal lattice and functional groups of hybrid BMP synthesize under different parameters were analyzed by X-ray diffraction (XRD) and Fourier transform infrared spectroscopy (FTIR). There are no obvious changes in functional groups, the full width at half maximum decreased as Ag NPs size increased at a reaction temperature of 80 °C (Additional file 1: Fig. S2). These
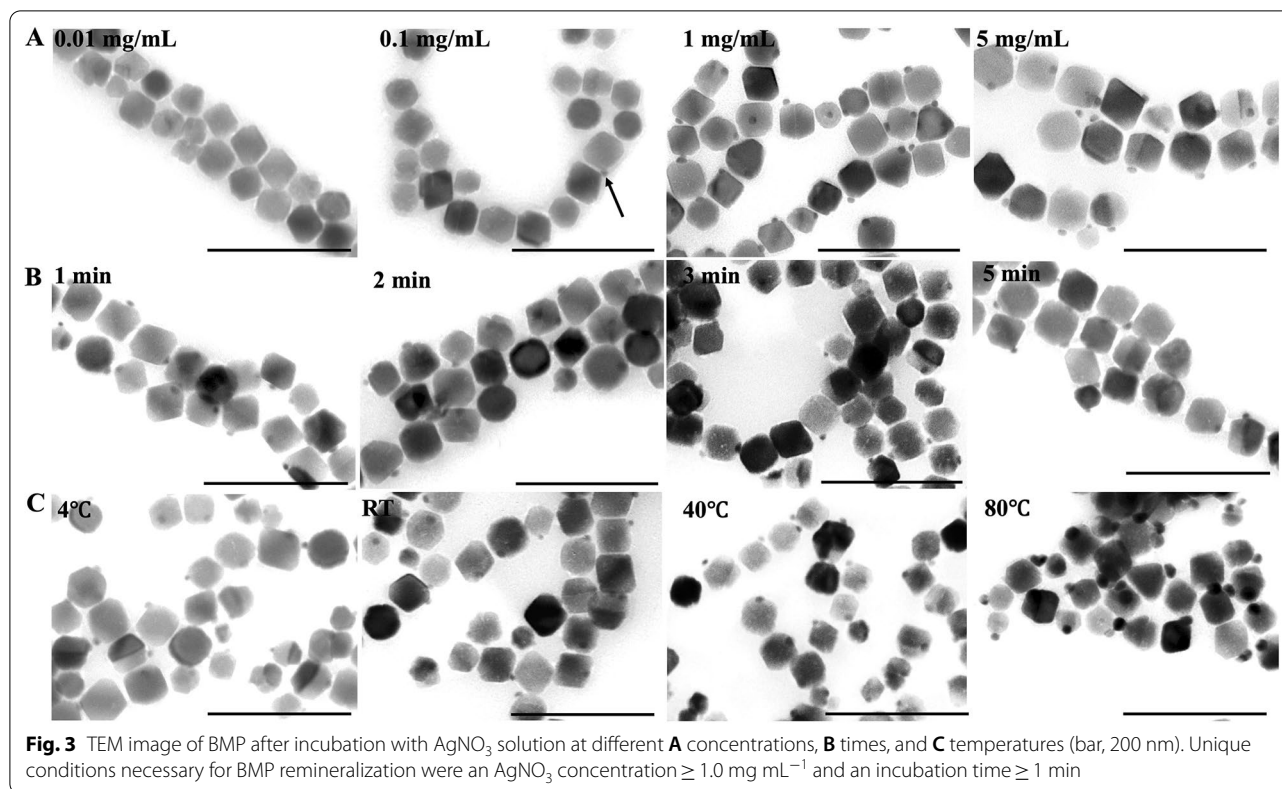
Xu *et al. Journal of Nanobiotechnology*   (2022) 20:364

Page 5 of 14

Fig. 2 **A** Transmission electron microscopy (TEM) image of BMP after incubation with Ag⁺. BMP was synthesized to form a novel nanocomposite with a Janus-like Ag-Fe₃O₄ core. **B**, **C** High-resolution transmission electron microscopy (HTEM) image of hybrid BMP and the interface between Ag and Fe₃O₄ crystals. Hybrid BMP was coated by an outer biomembrane (black arrow). Ag and Fe₃O₄ lattice were staggered with each other at the interface and formed a whole Ag-Fe₃O₄ core. **D** TEM image of the hybrid BMP after removing the biomembrane, Ag NPs did not separate from the Fe₃O₄ crystals. **E** HAADF-STEM image and element mapping of Fe and Ag in the hybrid BMP. **F** EDS spectra of Ag NPs of hybrid BMP. **G** XPS patterns of Ag-Fe₃O₄ hybrid BMP and BMP. Corresponding particles size distributions of (**H**) Ag NPs of hybrid BMP

results indicated that the unique conditions necessary for BMP remineralization were an AgNO$_3$ concentration ≥ 1.0 mg mL^{-1} and an incubation time ≥ 1 min.

The magnetotactic bacteria MSR-1 cannot synthesize Ag-Fe₃O₄ hybrid BMP under these conditions (Additional file 1: Fig. S3) owing to no Ag efflux pump on the MSR-1 cell membrane. Different chemical syntheses Fe₃O₄ NPs and commercial magnetic particles cannot synthesize Ag NPs either under these conditions (Additional file 1: Fig. S4). The remineralization just happened on BMPs. Chemical synthesis of Ag-Fe₃O₄ hybrids always was a complex process, requiring a catalyst, protective agent, high-temperature, and pressure equipment [46, 47]. The remineralization of BMP at mild pH, pressure, and temperature, did not entail toxic or hazardous substances, and avoided of the addition of external reducing, capping, and stabilizing agents. Thus the remineralization of BMP provided a straightforward and green method to prepare Ag-Fe₃O₄ hybrids.

Antimicrobial activity of hybrid BMPs

Wound infections caused by bacteria leading to unsuccessful wound healing is one of serious health problems.

Ag NPs display good antibacterial activity [36] and noble-metal-magnetic heterostructures can prevent Ag⁺ release rate from the cathodic Ag, reducing the cytotoxicity of Ag [48]; therefore, Ag-Fe₃O₄ hybrid BMP and biofilm removed hybrid BMP (Ag-Fe₃O₄ hybrids) can be an ideal wound dressing materials. First, we detected the activities of hybrid BMP and Ag-Fe₃O₄ NPs against bacteria by the spot test, with commercial Ag NPs as the positive control and BMP as the negative control. The bacteria *E. coli* (representative of gram-negative bacteria), *S. aureus* (representative of gram-positive bacteria), and *P. aeruginosa*, which can cause several serious infections, were selected to perform the experiments (Fig. 4A). After 12 h of exposure, Ag-Fe₃O₄ NPs at a concentration of 2.0 mg mL^{-1} inhibited the growth of *E. coli*, *S. aureus* and *P. aeruginosa*. The antibacterial activity of Ag-Fe₃O₄ NPs increased with time, and the antibacterial effect of 1.0 mg mL^{-1} of Ag-Fe₃O₄ NPs was observed following 24 h of exposure. Ag-Fe₃O₄ NPs presented comparable results with commercial Ag NPs. However, hybrid BMP displayed antibacterial activity at a concentration of 2.0 mg mL^{-1} after 24 h of exposure; the antibacterial activity was lower than those of Ag-Fe₃O₄ and Ag NPs.

Xu *et al. Journal of Nanobiotechnology*   (2022) 20:364

Page 6 of 14

Fig. 3 TEM image of BMP after incubation with $AgNO_3$ solution at different **A** concentrations, **B** times, and **C** temperatures (bar, 200 nm). Unique conditions necessary for BMP remineralization were an $AgNO_3$ concentration $\geq$ 1.0 mg mL^{-1} and an incubation time $\geq$ 1 min

This may be owing to the biomembrane of hybrid BMP prevent the release rate of Ag$^+$. BMP NPs had no inhibitory effect on *E. coli*, *S. aureus* and *P. aeruginosa* even up to the highest test concentration of 2.0 mg mL^{-1}. Those results indicated that hybrid BMP and Ag-Fe$_3$O$_4$ NPs all displayed good antibacterial activity.

The antibacterial activities of BMP-Ag and Ag-Fe$_3$O$_4$ NPs were compared with commercially available antibiotics ampicillin(Amp) and gentamicin(Gm). BMP-Ag and Ag-Fe$_3$O$_4$ NPs displayed better antibacterial activity than ampicillin and gentamicin. There are no colonies formed of *S. aureus*, *E. coli*, and *P. aeruginosa* after treatment with BMP-Ag and Ag-Fe$_3$O$_4$ NPs (Fig. 4B, D, F). The antibacterial activity of BMP-Ag and Ag-Fe$_3$O$_4$ reached 100%, significantly higher than ampicillin 90% for *S. aureus* (Fig. 4C), and than ampicillin 61% and gentamicin 85% for *P. aeruginosa* (Fig. 4G). Antibiotics are selective in their antibacterial properties, e.g. ampicillin has a low antibacterial activity to *P. aeruginosa* and always requires combined use of antibiotics [49–51]. Nanomaterials possess broad-spectrum antibacterial properties and can inhibit all test pathogenic.
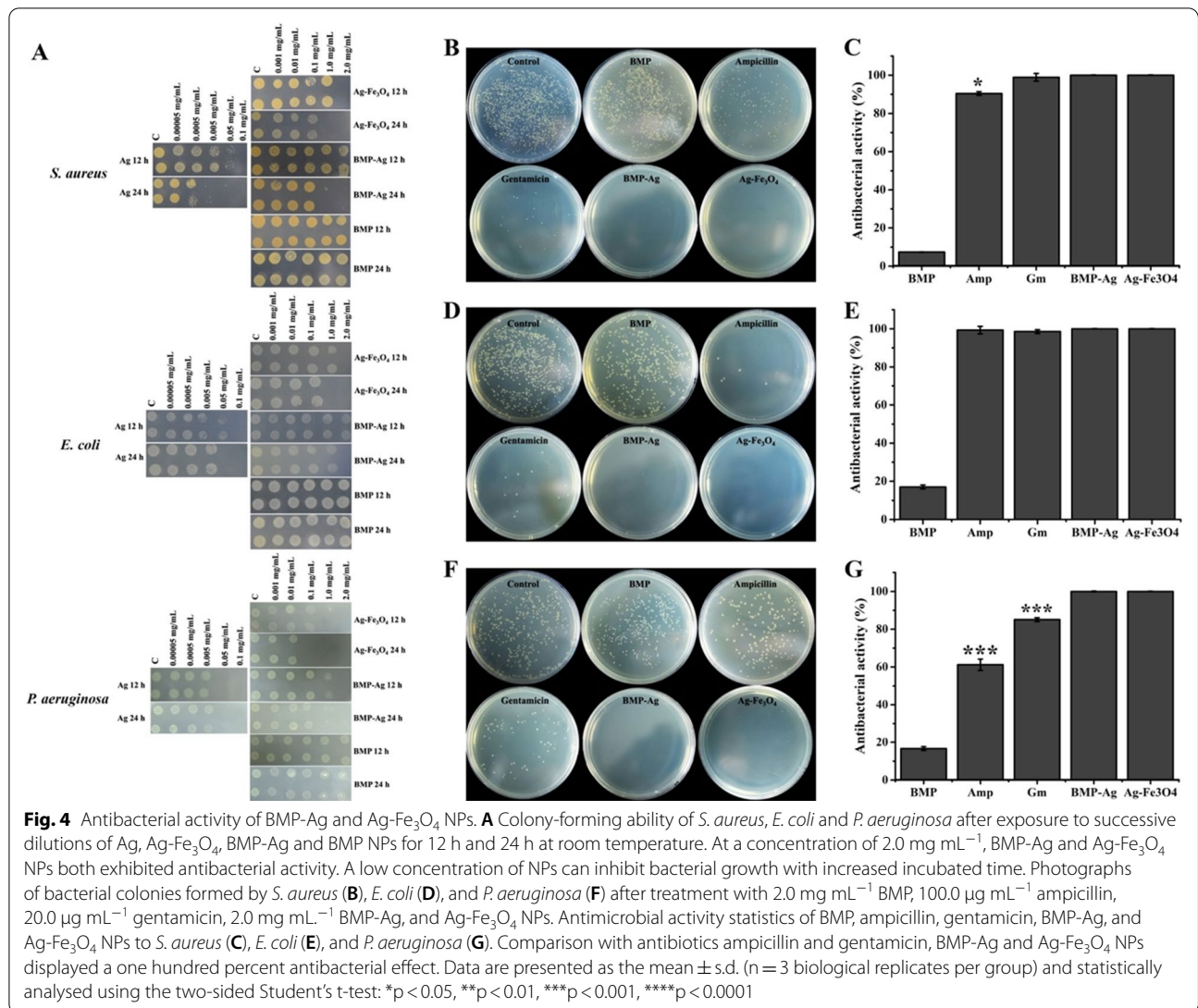
Biosafety evaluation of hybrid BMPs
Additionally, the cytotoxicity of BMP-Ag and Ag-Fe$_3$O$_4$ NPs to mouse fibroblast cell line (L929) and normal human liver cell line (LO2) were detected and compared with those of Ag NPs and BMP using Cell Counting Kit-8 and Calcein-AM/PI kit. As shown in Fig. 5A, B, BMP-Ag and Ag-Fe$_3$O$_4$ NPs exhibited lower cytotoxicity in the two cell lines than Ag NPs at the same Ag concentration. The cell viability of L929 (Fig. 5A) and LO2 (Fig. 5B) treated with 1000 μg mL^{-1} of BMP-Ag and Ag-Fe$_3$O$_4$ NPs decreased to approximately 88.1% and 75.7%, and 80.2% and 76%, respectively. The cell viability of L929 and LO2 treated with Ag NPs decreased to approximately 65.2% and 50%, respectively. Even up to the highest test concentration of 1000 μg mL^{-1}, BMP was not cytotoxic to the two cell lines. The Calcein-AM/PI cell stain results at the highest test concentration are shown in Fig. 5C; there are fewer red-fluorescent cells (dead cells) in the groups treated with Ag-Fe$_3$O$_4$, BMP-Ag, and BMP NPs than in those groups treated with Ag NPs (Fig. 5C). These findings indicated that hybrid BMP and Ag-Fe$_3$O$_4$ NPs have lower cytotoxicity and good biocompatibility to normal mouse and human cell lines and can be used in biomedical applications.

In vivo wound healing of hybrid BMP
Based on the above results, hybrid BMP and relevant Ag-Fe$_3$O$_4$ NPs showed efficient antibacterial activity and lower cell cytotoxicity; therefore, they are suitable biomaterials against bacterial wound infection.
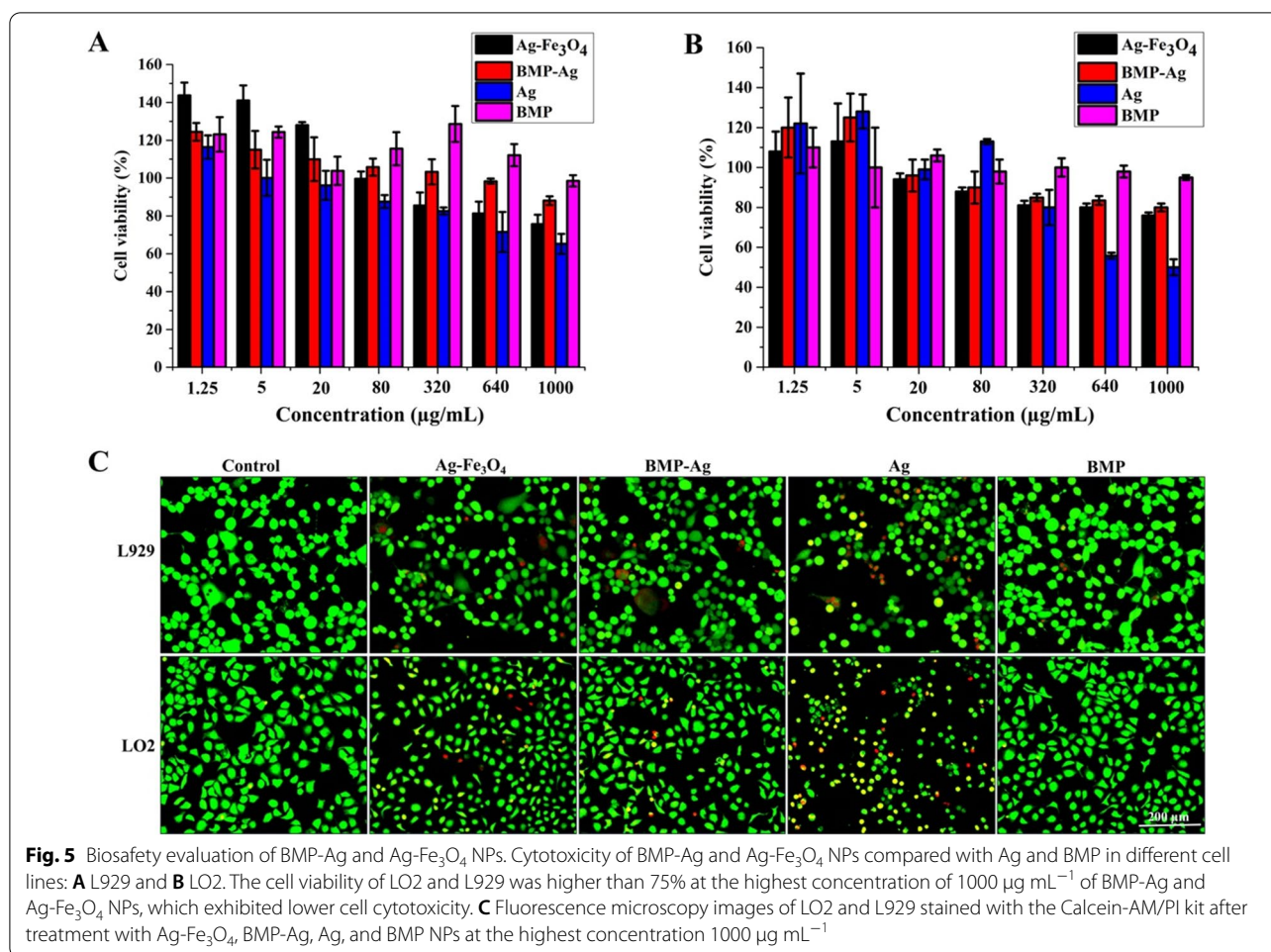
Xu *et al. Journal of Nanobiotechnology*   (2022) 20:364

Page 7 of 14

Fig. 4 Antibacterial activity of BMP-Ag and Ag-Fe$_3$O$_4$ NPs. **A** Colony-forming ability of *S. aureus*, *E. coli* and *P. aeruginosa* after exposure to successive dilutions of Ag, Ag-Fe$_3$O$_4$, BMP-Ag and BMP NPs for 12 h and 24 h at room temperature. At a concentration of 2.0 mg mL^{-1}, BMP-Ag and Ag-Fe$_3$O$_4$ NPs both exhibited antibacterial activity. A low concentration of NPs can inhibit bacterial growth with increased incubated time. Photographs of bacterial colonies formed by *S. aureus* (**B**), *E. coli* (**D**), and *P. aeruginosa* (**F**) after treatment with 2.0 mg mL^{-1} BMP, 100.0 µg mL^{-1} ampicillin, 20.0 µg mL^{-1} gentamicin, 2.0 mg mL^{-1} BMP-Ag, and Ag-Fe$_3$O$_4$ NPs. Antimicrobial activity statistics of BMP, ampicillin, gentamicin, BMP-Ag, and Ag-Fe$_3$O$_4$ NPs to *S. aureus* (**C**), *E. coli* (**E**), and *P. aeruginosa* (**G**). Comparison with antibiotics ampicillin and gentamicin, BMP-Ag and Ag-Fe$_3$O$_4$ NPs displayed a one hundred percent antibacterial effect. Data are presented as the mean $\pm$ s.d. (n = 3 biological replicates per group) and statistically analysed using the two-sided Student's t-test: *$p < 0.05$, **$p < 0.01$, ***$p < 0.001$, ****$p < 0.0001$

Firstly, a round full-thickness open-excision wound was made on the mice's back and was infected with 500 µL (2×10^8 mL^{-1}) *S. aureus*. Then Ag-Fe$_3$O$_4$ hybrid BMP or Ag-Fe$_3$O$_4$ NPs were suspended in saline solution, and 80 µL 1.0 mg mL^{-1} Ag-Fe$_3$O$_4$ /Ag-Fe$_3$O$_4$ was smeared on the wound to treat the infected wound; the treatment process is shown in schematic diagram Fig. 6A. The therapeutic efficacy was compared with Ag NPs, BMP, and saline (control) treatment groups. The Ag-Fe$_3$O$_4$ NPs showed enhanced wound contraction compared with Ag, BMP-Ag, BMP, and the control. On day 7, the wounds of Ag-Fe$_3$O$_4$ NP-treated mice healed almost completely (Fig. 6B). The rate of wound closure was 88%, which was significantly higher than those of the control group with 75%, BMP group with 76%, and Ag NP group with 80% (Fig. 6C). The rates of bacterial death under a scab of the

hybrid BMP, Ag-Fe$_3$O$_4$, Ag, and BMP groups were significantly higher than that of the control group (Fig. 6D). As the treatment time increased, the biomembrane of BMP degraded, showing weak antibacterial activity. Different treated tissue sections were stained with hematoxylin–eosin (H&E) on day 7. The Ag-Fe$_3$O$_4$ treated infected wound showed obvious tissue regeneration and almost no inflammation compared to control (Fig. 6E). With the antibacterial activity of Ag NPs and Fe$_3$O$_4$, Ag-Fe$_3$O$_4$ NPs displayed better therapeutic efficacy.

Conclusion

To the best of our knowledge, we are the first to report a simple and green method to synthesise BMP-Ag and Fe3O4-Ag NPs through BMP-mediated growth. By mixing BMP with AgNO3 solution of $\geq$ 1.0 mg/mL, noble metal–magnetic nanohybrids were quickly synthesised

Xu *et al. Journal of Nanobiotechnology* (2022) 20:364

Page 8 of 14

Fig. 5 Biosafety evaluation of BMP-Ag and Ag-Fe$_3$O$_4$ NPs. Cytotoxicity of BMP-Ag and Ag-Fe$_3$O$_4$ NPs compared with Ag and BMP in different cell lines: **A** L929 and **B** LO2. The cell viability of LO2 and L929 was higher than 75% at the highest concentration of 1000 µg mL^{-1} of BMP-Ag and Ag-Fe$_3$O$_4$ NPs, which exhibited lower cell cytotoxicity. **C** Fluorescence microscopy images of LO2 and L929 stained with the Calcein-AM/PI kit after treatment with Ag-Fe$_3$O$_4$, BMP-Ag, Ag, and BMP NPs at the highest concentration 1000 µg mL^{-1}

within 1 min. Despite the rapid synthesis process, the produced BMP-Ag was stable; therefore, large production of BMP-Ag and Fe3O4-Ag NPs is possible through magnetotactic bacteria fermenter cultivation. BMP-Ag and Fe3O4-Ag NPs displayed good biocompatibility and antibacterial activity and can be used to treat infected wounds. Compared with the chemical synthesis of Ag-Fe3O4 NPs, the synthesis method of BMP-Ag NPs is simple and eco-friendly. BMP-Ag NPs are enveloped by a BMP membrane, which can be easily modified with proteins, nucleic acids, and anticancer drugs and used as a nanocarrier in tumors diagnosis and treatment.
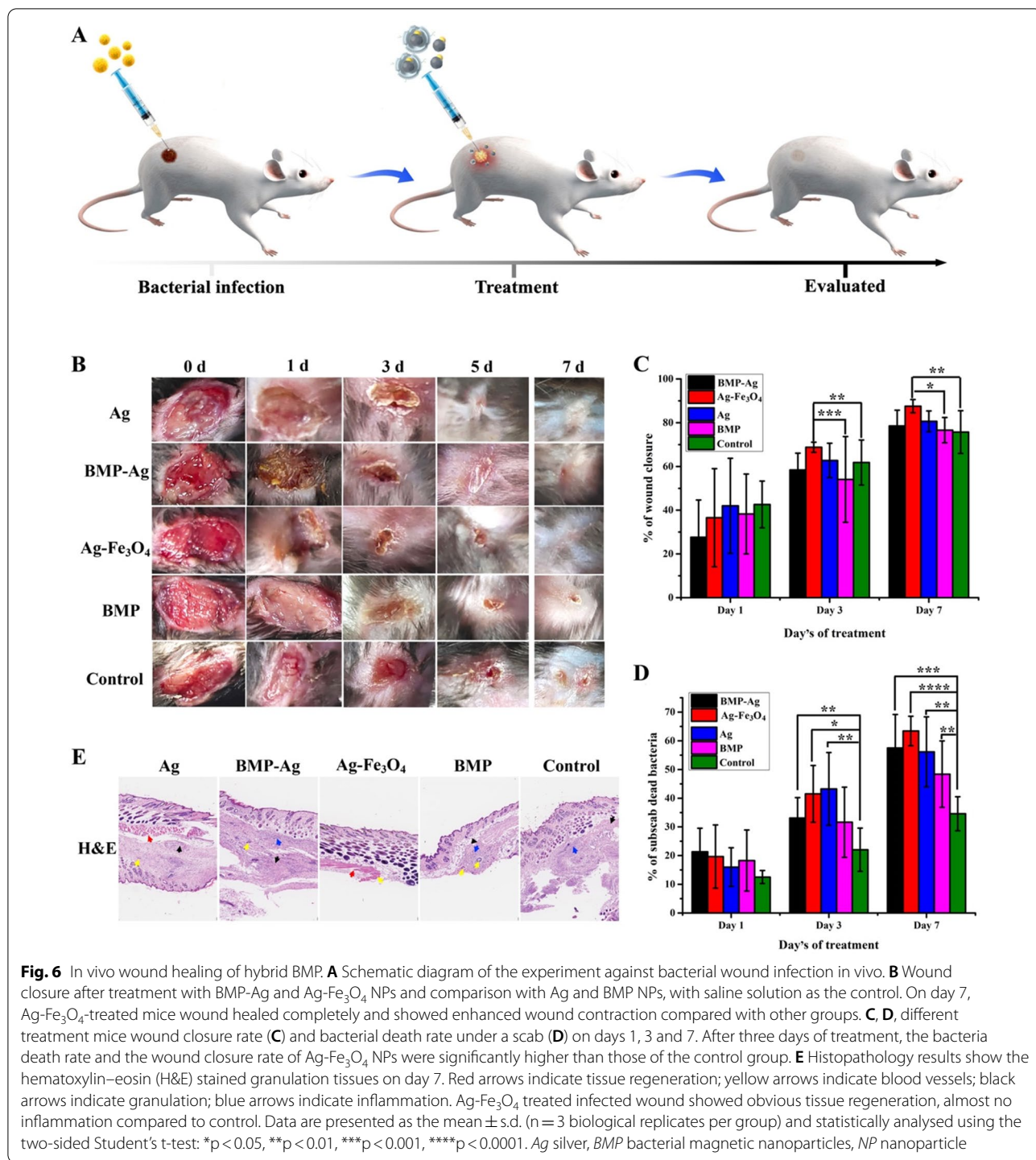
Our findings represent a significant improvement in BMP properties and facilitate the biosynthesis of multifunctional heterogeneous hybrid BMP. BMP acted as an active nano-sized biological reaction kettle in the remineralization process, mineralizing the ions (e.g., Ag$^+$) entering the BMP membrane. The proposed approach could lead to the dawn of a new type of biosynthesis technology, potentially mineralizing numerous metal ions or

loading drugs into the BMP to synthesize a wider range of multifunctional biomaterials.

Discussion

Multidrug resistant microorganisms are considered a major health problem worldwide with increasing mortality and morbidity, which raises the need to search for alternative methods of controlling antibiotic-resistant pathogens [52]. Various nanoparticles have made remarkable progress with their promising antibacterial activity in a wide range of bacteria [53]. Among these, silver nanoparticles (Ag-NPs) exert robust, broad-spectrum antimicrobial efficacy through multiple and simultaneous mechanisms and are relatively free of adverse effects. They can increase the permeability of cell membranes, produce reactive oxygen species, interrupt replication of deoxyribonucleic acid, and destroying biofilm by releasing silver ions [54]. Ag-NPs have already been successfully applied in various biomedical and antimicrobial technologies and products used in everyday life [55]. However, the Ag accumulation in the human body

Xu *et al. Journal of Nanobiotechnology*   (2022) 20:364

Page 9 of 14

Fig. 6 In vivo wound healing of hybrid BMP. **A** Schematic diagram of the experiment against bacterial wound infection in vivo. **B** Wound closure after treatment with BMP-Ag and Ag-Fe$_3$O$_4$ NPs and comparison with Ag and BMP NPs, with saline solution as the control. On day 7, Ag-Fe$_3$O$_4$-treated mice wound healed completely and showed enhanced wound contraction compared with other groups. **C**, **D**, different treatment mice wound closure rate (**C**) and bacterial death rate under a scab (**D**) on days 1, 3 and 7. After three days of treatment, the bacteria death rate and the wound closure rate of Ag-Fe$_3$O$_4$ NPs were significantly higher than those of the control group. **E** Histopathology results show the hematoxylin–eosin (H&E) stained granulation tissues on day 7. Red arrows indicate tissue regeneration; yellow arrows indicate blood vessels; black arrows indicate granulation; blue arrows indicate inflammation. Ag-Fe$_3$O$_4$ treated infected wound showed obvious tissue regeneration, almost no inflammation compared to control. Data are presented as the mean ± s.d. (n = 3 biological replicates per group) and statistically analysed using the two-sided Student's t-test: *p < 0.05, **p < 0.01, ***p < 0.001, ****p < 0.0001. *Ag* silver, *BMP* bacterial magnetic nanoparticles, *NP* nanoparticle

and environments showed toxic effects when it deposits to a certain amount [56, 57]. Bacteria can also develop resistance to silver nanoparticles after repeated exposure [58]. Magnetic composites, such as Ag-Fe$_3$O$_4$, are a new generation of magnetic antimicrobial NPs, which facilitate local distribution, targeted delivery, and tissue

penetration [59, 60]. Targeted delivery reduces bacteria's exposure time and opportunity to Ag, thereby decreasing the speed by which the pathogen develops resistance and benefiting the removal or retrieval of Ag-NPs [61].

Both Ag-NPs and Fe$_3$O$_4$ NPs have been intensively studied in wound healing. Besides antibacterial activity,

Xu *et al. Journal of Nanobiotechnology*   (2022) 20:364

Page 10 of 14

Ag-NPs also possess an anti-inflammatory effect, which made them play a role in the wound healing process by inhibiting the synthesis of tumour necrosis factor [TNF]-α, interferons, and interleukin 1 that involved in inflammatory processes [62]. The functional role of iron in the wound healing process has not been fully understood. Recent interests focused on lactoferrin, an iron-binding glycoprotein secreted from glandular epithelial cells [63]. The protein promotes cutaneous wound healing by enhancing the initial inflammatory phase, and cell proliferation and migration. When treated with lactoferrin, human keratinocytes, fibroblasts and endothelial cells migrate and invade more rapidly in vitro. And the in vivo analysis proved that lactoferrin favoured the closure of skin wounds performed on the mice back [64]. Fe_3O_4 NPs were reported to sustained release trace amount of ferric and ferrous ions to their environments [65], thus help to keep the iron homeostasis around wound, and accelerated wound closure, reduced scar width, and enhanced angiogenesis [66]. The composite nanoparticle, $Ag-Fe_3O_4$, simultaneously provided properties of both above NPs in wound healing [65].

MTBs synthesize BMPs and their magnetic crystal cores under mild physiological conditions and strict genetic control. The whole process is a unique and promising platform in the intracellular fabrications of nanomaterials [67]. However, very few materials have been made through this platform. Most studies interests are focused on the direct utilization or surface modification of BMP particles [68]; few have tried to change the composition and shapes of BMP crystals, and only trace amounts of exogenous elements could be incorporate into BMP crystals [29]. Thus, innovative methods are necessary to synthesise engineered BMPs with various compositions and shapes for wider application. Here, we constructed an Ag/Fe_3O_4 nanostructure, one of the most important binary systems in recent research hot spots of nanotechnology [69].

Most researchers instinctively thought that purified BMPs were the end products of nanomaterials. However, BMPs contained excess ferrous ions inside MM [23], active proteins and lipids [70]. These components could act as reducing agents and facilitate further synthesis of BMP core crystals even in vitro. For example, ions of noble metals such as silver, gold, and platinum have higher electric potentials than ferrous ions, when transferred into BMP vesicles by diffusion. Thus, they could oxidize ferrous ions and crystalize on the surface of BMP core crystals (Fig. 7D). This process led to the formation of Janus-like BMP-Ag NPs, and the original ferrous ions lost their outer-shell electrons and doped into BMP crystals. Content of Fe_2O_3 in the samples increased from 26.2% to 40.9% after remineralization (Fig. 7AB). The average diameter of BMP central crystals was slightly

Fig. 7 XPS analysis of Fe_3O_4 and Fe_2O_3 contents of **A** hybrid BMP and **B** BMP. **C** Fe_3O_4 diameter statistical distribution of BMP and $Ag-Fe_3O_4$ hybrid BMP. **D** Schematic diagram of BMP-Ag NP synthesis. Ag^+ is transported into the BMP membrane. The Fe(II) inside the BMP membrane gives an electron to Ag^+, Ag^+ is reduced and nucleated, and Ag NPs are formed on one crystal plane of Fe_3O_4. Fe(II) that loses an electron was oxidized until biomineralization

Xu *et al. Journal of Nanobiotechnology*   (2022) 20:364

Page 11 of 14

increased from 42.29 ± 6.78 nm to 43.14 ± 6.34 nm (Fig. 7C). However, we found that the Cu/Ag efflux pump *MGMSRv2_1436* protein only exists on BMP membrane (Additional file 1: Table S1) and constructed the *MGM-SRv2_1436* mutant strain MSR-Δ*1436* (Additional file 1: Fig. S5). The BMP of MSR-Δ*1436* still mineralized Ag^+ to form Ag NPs(Additional file 1: Fig. S6), but Ag NPs could not be synthesized by individual Fe_3O_4 crystals or BMP membrane(Additional file 1: Fig. S7). The synergy between the biomembrane, Fe_3O_4 crystal, and unmineralized iron enabled the remineralization of BMPs. Although BMP displayed bioactivity, it was different from the organism. The mechanisms of BMP remineralization need further investigation.

This work successfully synthesized a new kind of BMPs with heterodimer cores. As the second step of the synthesis was occurred in BMP vesicles, we suggest that BMP was not only just a nanomaterial composite, but also an active biological reaction kettle in nano size.

Experimental section

Magnetospirillum gryphiswaldense MSR-1 fermentation culture: *M. gryphiswaldense* MSR-1 was cultured in a 42-L fermenter (BioFlo110; New Brunswick Scientific, NJ, USA) as described previously [71]. A 5-mL inoculum was activated in 45 mL of fresh sodium lactate medium at 30 °C/100 rpm. Subsequently, MSR-1 was subjected to three sequential transfers, and the third inoculum (3 L) was transferred to a 42-L fermenter. The fermenter had a working volume of 30 L (3 L of inoculum and 27 L of fermentation medium), and the fermentation initial airflow and agitation were set at 0.5 L/min and 100 rpm, respectively. Once the level of dissolved oxygen ($dO_2\%$) decreased to approximately 15%, airflow was increased to 1.0 L/min. The fermentation $dO_2\%$ level continuously decreased with bacterial growth. Once the dO2% level decreased to approximately 1%, agitation was increased to 10 rpm every 2 h to maintain anaerobic condition. The pH of the fermenter was maintained at 6.8 by automated addition of a lactic acid feeding medium. MSR-1 OD_{565} and magnetic response (Cmag value) were measured during fermentation. Once the Cmag value decreased to approximately 0.8, fermentation was terminated. Cells were collected by centrifugation at 8000 rpm for 10 min and then stored at -80 °C to purify the BMP.

Purification of BMPs: MSR-1 cells were suspended in 50 mmol L^{-1} of phosphate-buffered saline (PBS) with a weight-to-volume ratio of 1:10 and then disrupted by ultrasonication (NingBo Scientz Biotechnology Co., Ltd., China) at 300 W for 30 min. Cellular debris was kept on a neodymium magnet at 4 °C overnight, and the supernatant was emptied. The BMP crude extract was left suspended

in 10 mmol L^{-1} of PBS buffer and washed by low-power ultrasonication (power, 200–80 W; operation time, 3 s; inter-arrival, 5 s; total time, 15 min every time) several times. After each wash, the suspended BMP was subjected to permanent magnet adsorption, and the protein concentration in the supernatant was detected on a UV–visible spectrophotometer (UNICO2100; UNICO Instrument Co., Shanghai, China). Pure BMPs were obtained until the protein concentration was < 0.1 mg mL^{-1}. BMPs were washed 3–5 times in deionised water using an ultrasonic cleaner to remove the remaining PO_4^{3-} and Cl^- and stored at 4 °C.

Remineralization of BMPs: fresh BMPs were mixed with $AgNO_3$ solution, incubated at room temperature, and then absorbed by a magnet. After removal of the supernatant, the precipitate was washed 3–5 times in deionized water, obtained Ag-Fe_3O_4 hybrid BMP, and stored at 4 °C.

The unique conditions necessary for BMP remineralization were determined by changing $AgNO_3$ concentration, incubation time, and temperature.

Janus-like Ag-Fe_3O_4 NPs can be made by removing the membrane of Ag-Fe_3O_4 hybrid BMP. Hybrid BMP was suspended in 10% sodium dodecyl sulphate and 3-M NaOH mixture, boiled for 10 min and then absorbed by magnet. The precipitate was suspended in deionised water and washed 3–5 times by ultrasonic cleaner; finally, Ag-Fe_3O_4 NPs were obtained.

Physicochemical characterisation of Ag-Fe_3O_4 hybrid BMPs: hybrid BMPs were characterised by X-ray photoelectron spectroscopy (XPS) (ESCALAB 250Xi, Thermo Fisher Scientific, MA, USA) and dark-field high-angle annular dark-field scanning transmission electron microscopy. The morphology and size of hybrid BMPs were analysed using high-resolution transmission electron microscopy (TEM) (JEOL USA, Inc., MA, USA). BMPs were used as a control.

Antibacterial activity of hybrid BMPs and Ag-Fe_3O_4 NPs: the antibacterial activities of hybrid BMPs and Ag-Fe_3O_4 NPs against gram-negative (*Escherichia coli*), gram-positive (*Staphylococcus aureus*) and *P. aeruginosa* bacteria were tested by a 'spot' assay, as described previously [72]. *E. coli*, *S. aureus*, and *P. aeruginosa* were cultured in 5 mL of a Luria–Bertani (LB) liquid medium at 37 °C 200 rpm^{-1}. Cell density OD_{600} was detected in the culture process, and OD_{600} reached approximately 0.5. The cell was collected, washed two times in deionised water, and suspended in 5 mL of ddH$_2$O. Subsequently, 100 µL suspensions of *E. coli*, *S. aureus*, and *P. aeruginosa* were incubated with successive dilutions of hybrid BMPs, Ag-Fe_3O_4 NPs, and BMP (2.0, 1.0, 0.1, 0.0, and 0.001 mg mL^{-1}) and Ag NPs (0.1, 0.05, 0.005, 0.0005, and 0.00005 mg mL^{-1}) in a 96-well microtiter plate at room temperature. After 12 and 24 h of incubation, 3 µL of cell suspension was added onto the

Xu *et al. Journal of Nanobiotechnology*   (2022) 20:364

Page 12 of 14

LB agar medium and incubated at 37 °C in a constant-temperature incubator for 10 h. The number of visible 'spots' formed (bacterial colonies) was recorded.

The antibacterial activity compare test of hybrid BMPs and antibiotics were tested by plate count method. The concentrations of antibiotics ampicillin and gentamicin were 100 μg/mL and 20 μg/mL, respectively, for the test, which is the most frequently used concentration in the Luria–Bertani medium. The 100 μL *E. coli*, *S. aureus*, and *P. aeruginosa* were coated one LB solid medium, after treatment with 2.0 mg mL^{-1} hybrid BMPs, Ag-Fe$_3$O$_4$ NPs and BMP, 0.1 mg mL^{-1} Ag NPs, 100.0 μg mL^{-1} ampicillin, and 20.0 μg mL^{-1} gentamicin, respectively. Then, they were cultured at 37 °C in a constant-temperature incubator for 12 h. The bacterial colonies were photographed and counted. The antibacterial activity (%) was calculated as (Ne-Nc)/Nc × 100, where Ne the number of colonies corresponding to the experiment group, and Nc the number of colonies to the control group.

Hybrid BMPs were pretreated with protein K to digest the protein on the biomembrane. Hybrid BMPs were suspended in protein K solution with a weight ratio of 1:1 and then incubated at 50 °C for 3 h. After digestion, hybrid BMPs were washed 3–5 times in deionized water using an ultrasonic cleaner.

Wound-healing activity of hybrid BMPs and Ag-Fe$_3$O$_4$ NPs: female C57 mice (20–25 g) aged 6–8 weeks were anaesthetised with 10% chloral hydrate (300 mg/kg) by intraperitoneal injection. Dorsal hair were shaved, and the shaved area was wiped with povidone-iodine. A round full-thickness open-excision wound (8 mm in diameter) was made and then smeared with 500 μL (2×10^8 mL^{-1}) of fresh *S. aureus* solution. After 1 day, 80 μL of 0.05 mg mL^{-1} Ag, 1.0 mg mL^{-1} hybrid BMPs, Ag-Fe$_3$O$_4$, and BMP were smeared on the wound. The control was smeared with 80 μL of saline solution. Wound healing was recorded by a camera, and the wound area was measured using Photoshop (Adobe Inc., CA, USA). The wound contraction rate was calculated as (original wound area − actual wound area)/original wound area × 100.

The number of bacterial colonies under a scab was counted at days 0, 1, 3 and 7. A 0.01 g of wound edge tissue was cut and homogenised in a micro-homogeniser with 100 mL of saline solution. Subsequently, the homogenate was diluted to 1:10^6 with saline solution, and 10 μL of the diluent was added onto the LB agar medium and incubated at 37 °C for 12 h. The number of bacterial colonies was counted, and the bacterial death rate under a scab was calculated as (original colonies − actual colonies)/original colonies × 100. All animal protocols were approved by the Biological and Medical Ethics Committee of Beihang University (Approval Number: BM20200087).

Data Analysis and Statistics: The "t-test" was conducted for all statistical analyses. The results are presented as mean ± standard deviation (SD). In all figures, * and ** denote that the p-value is less than 0.05 and 0.01, respectively. All experiments were repeated independently at least three times.

Supplementary Information

The online version contains supplementary material available at https://doi.org/10.1186/s12951-022-01532-4.

Additional file 1: Figure S1. Ag nanoparticle diameter statistical distribution of Ag-Fe$_3$O$_4$ hybrid BMPs synthesis at room temperature and 80℃. The average diameter of Ag nanoparticles was 9.85±2.22 nm and 17.51±3.14 nm under room temperature and 80℃, which increased almost two fold. **Figure S2.** Functional groups and crystal lattice analysis of BMP-Ag synthesized under AgNO$_3$ concentration 1.0 mg/mL, reaction time 1 min, reaction temperature 80℃, and room temperature by FTIR and XRD. The functional groups of BMP-Ag no obvious change under different synthesized parameters. There is a faint diffraction peak at 38.1° of BMP-Ag responding to the (111) crystal plane of face-centered cubic Ag compared with BMP, and the full width at half maximum decreased as the Ag NP size increased at a reaction temperature of 80 °C. **Figure S3.** (A) Magnetotactic bacteria MSR-1 cultured at different concentrations of AgNO$_3$ solution. The bacterial growth was inhibited when the AgNO$_3$ concentrations >1.0 mg/mL. (B) Transmission electron microscopy image of MSR-1 cultured under 1.0 mg/mL AgNO$_3$ solution. There is no synthesis of Ag-Fe$_3$O$_4$ hybrid BMP. **Figure S4.** Transmission electron microscopy image of chemically synthesized Fe$_3$O$_4$(A), commercial biotinylated magnetic beads(B), and streptavidin magnetic beads(C) and BMPs(D) after incubating with AgNO$_3$ solution. Only BMP can mineralize Ag$^+$ into Ag nanoparticles. **Figure S5.** Construction of *MGMSRv2_1436* gene deletion mutant. (A) Schematic diagram of the construction of suicide vector pUXcusA. (B) Amplified upstream and downstream fragments of *MGMSRv2_1436* gene and gentamicin resistance cassette gene. (C) Polymerase chain reaction (PCR) amplified the internal gene of *MGMSRv2_1436* (*1436*), gentamicin resistance gene (Gm), upstream and downstream fragments of *MGMSRv2_1436* gene to confirm the screened *MGMSRv2_1436* mutant strain. #: *MGMSRv2_1436* mutant strain, + WT MSR-1 positive control, - ddH2O negative control. There was no *MGMSRv2_1436* gene, but has gentamicin resistance gene, upstream, and downstream fragments in the screened colonies, mean *MGMSRv2_1436* deletion mutant was obtained successfully. (D) PCR amplified the genes (*mamB, mamD, mamE, mamO, mamX, mamZ, mms6, feoB*) associated with the magnetosome synthesis. It was confirmed that no genes were lost in the construction process. **Figure S6.** Transmission electron microscopy image of MSR-Δ*1436* BMP after incubating with AgNO$_3$ solution. MSR-Δ*1436* BMP still can mineralize Ag$^+$ into Ag nanoparticles; it was indicated that Ag$^+$ transported into BMP membrane did not base on efflux pump MGMSRv2_1436 protein *in vitro* state. **Figure S7.** Transmission electron microscopy image of Fe$_3$O$_4$ crystal and vesicle(B) of BMP after incubating with AgNO$_3$ solution. There is no Ag nanoparticle was synthesis on those two components. It was indicated that remineralization of BMP needs synergy of each element of BMP. **Table S1**. Proteins of only exist on BMP membrane.

Author contributions

JX, JT, and LF conceived and designed the experiments. JX, SM, LJ, XB, HS, and HZ performed the experiments. JX, FL, WZ, CC, and LF analyzed the data. JX, FA and JT drafted and wrote the manuscript. TZ detected EDS of hybrid BMP. LQ analyzed the elements of hybrid BMP. All authors read and approved the final manuscript.

Xu *et al. Journal of Nanobiotechnology*   (2022) 20:364

Page 13 of 14

Availability of data and materials

All datasets are available upon reasonable request.

Declarations

Ethics approval and consent to participate

All animal protocols were approved by the Biological and Medical Ethics Committee of Beihang University (Approval Number: BM20200087).

Consent for publication

Not applicable.

Competing interests

The authors declare that they have no competing interests.

Author details

[1]School of Mechanical Engineering and Automation, Beihang University, Beijing 100083, China. [2]State Key Laboratory of Agrobiotechnology, College of Biological Sciences, China Agricultural University, Beijing 100193, China. [3]State Key Laboratory of Ophthalmology, School of Biomedical Engineering, Wenzhou Medical University, 270 Xueyuanxi Road, Wenzhou 325027, China. [4]Key Laboratory of Earth and Planetary Physics, Institute of Geology and Geophysics, Chinese Academy of Sciences, Beijing 100029, China. [5]Beijing Key Laboratory of Bioelectromagnetism, Institute of Electrical Engineering, Chinese Academy of Sciences, Beijing 100190, People's Republic of China. [6]College of Life Science, Huaibei Normal University, Huaibei 235000, China. [7]Department of Mechanical Engineering, The University of Tokyo, Tokyo 113-8656, Japan.

References

1. Ridgwell A, Zeebe R. The role of the global carbonate cycle in the regulation and evolution of the Earth system. Earth Planet Sci Lett. 2005;234(3–4):299–315.
2. Blackmore R. Magnetotactic bacteria. Science. 1975;190:377–9.
3. Amor M, Busigny V, Louvat P, Gélabert A, Cartigny P, Durand-Dubief M, Ona-Nguema G, Alphandéry E, Chebbi I, Guyot F. Mass-dependent and -independent signature of Fe isotopes in manetotactic bacteria. Science. 2016;352:705–8.
4. Frankel RB. Magnetic guidance of organisms. Annu Rev Biophys Bioeng. 1984;13:85–103.
5. Frankel RB, Blackmore RP, Torres De Araujo FF, Danon J. Magnetotactic bacteria at the geomagnetic equator. Science. 1981;212:1269–70.
6. Blakemore RP. Magnetotactic bacteria. Science. 1982;36:217–38.
7. Imlay JA. Pathways of oxidative damage. Annu Rev Microbiol. 2003;57:395–418.
8. Byrne JM, Klueglein N, Pearce C, Rosso KM, Appel E, Kappler A. Redox cycling of Fe(II) and Fe(III) in magnetite by Fe-metabolizing bacteria. Science. 2015;347:1473–6.
9. Guo FF, Yang W, Jiang W, Geng S, Peng T, Li JL. Magnetosomes eliminate intracellular reactive oxygen species in *Magnetospirillum gryphiswaldense* MSR-1. Environ Microbiol. 2012;14(7):1722–9.
10. Li K, Chen C, Chen C, Wang Y, Wei Z, Pan W, et al. Magnetosomes extracted from *Magnetospirillum magneticum* strain AMB-1 showed enhanced peroxidase-like activity under visible-light irradiation. Enzyme Microb Technol. 2015;72:72–8.
11. Schuerle S, Soleimany AP, Yeh T, Anand GM, Haberli M, Fleming HE, et al. Synthetic and living micropropellers for convection-enhanced nanoparticle transport. Sci Adv. 2019;5(4):eaav4803.
12. Felfoul O, Mohammadi M, Taherkhani S, de Lanauze D, Zhong XuY, Loghin D, et al. Magneto-aerotactic bacteria deliver drug-containing nanoliposomes to tumour hypoxic regions. Nat Nanotechnol. 2016;11(11):941–7.
13. Xing J, Yin T, Li S, Xu T, Ma A, Chen Z, et al. Sequential magneto-actuated and optics-triggered biomicrorobots for targeted cancer therapy. Adv Funct Mater. 2020. https://doi.org/10.1002/adfm.202008262.
14. Taherkhani S, Mohammadi M, Daoud J, Martel S, Tabrizian M. Covalent binding of nanoliposomes to the surface of magnetotactic bacteria for the synthesis of self-propelled therapeutic agents. ACS Nano. 2014;8(5):5049–60.
15. Xu J, Liu L, He J, Ma S, Li S, Wang Z, et al. Engineered magnetosomes fused to functional molecule (protein A) provide a highly effective alternative to commercial immunomagnetic beads. J Nanobiotechnol. 2019;17(1):37.
16. He J, Tian J, Xu J, Wang K, Li J, Gee SJ, et al. Strong and oriented conjugation of nanobodies onto magnetosomes for the development of a rapid immunomagnetic assay for the environmental detection of tetrabromobisphenol-A. Anal Bioanal Chem. 2018;410(25):6633–42.
17. Xiang Z, Yang X, Xu J, Lai W, Wang Z, Hu Z, et al. Tumor detection using magnetosome nanoparticles functionalized with a newly screened EGFR/HER2 targeting peptide. Biomaterials. 2017;115:53–64.
18. Wang C, Xu C, Zeng H, Sun S. Recent progress in syntheses and applications of Dumbbell-like nanoparticles. Adv Mater. 2009;21(30):3045–52.
19. Maddinedi SB. Green synthesis of Au-Cu2-xSe heterodimer nanoparticles and their in-vitro cytotoxicity, photothermal assay. Environ Toxicol Pharmacol. 2017;53:29–33.
20. Kuo TR, Hung ST, Lin YT, Chou TL, Kuo MC, Kuo YP, et al. Green synthesis of InP/ZnS core/shell quantum dots for application in heavy-metal-free light-emitting diodes. Nanoscale Res Lett. 2017;12(1):537.
21. Martins LHS, Rai M, Neto JM, Oliveira JAR, Martins JHS, Komesu A, Debora Moreira KT, Gomes PWP. Nanomaterials: properties, toxicity, safety, and drug delivery. In: Rai M, Santos CA, editors. Nanotechnology applied to pharmaceutical technology. Springer: Cham; 2017. p. 363–81.
22. Tri PN, Ouellet-Plamondon C, Rtimi S, Assadi AA, Nguyen TA. Methods for synthesis of hybrid nanoparticles. In: Mohapatra S, Nguyen TA, Nguyen-Tri P, editors. Noble metal-metal oxide hybrid nanoparticles: fundamentals and applications. Woodhead Publishing: UK; 2018. p. 3–6.
23. Barabadi H. Nanobiotechnology: a promising scope of gold biotechnology. Cell Mol Biol (Noisy-le-grand). 2017;63(12):3–4.
24. Soni V, Raizada P, Singh P, Cuong HN, Rangabhashiyam S, Saini A, et al. Sustainable and green trends in using plant extracts for the synthesis of biogenic metal nanoparticles toward environmental and pharmaceutical advances: a review. Environ Res. 2021;202: 111622.
25. Saravanan M, Barabadi H, Vahidi H. Green nanotechnology: isolation of bioactive molecules and modified approach of biosynthesis. In: Patra C, Ahmad I, Ayaz M, Khalil AT, Mukherjee S, Ovais M, editors. Biogenic nanoparticles for cancer theranostics. Asterdam: Elsevier Inc; 2021.
26. Marcano L, Muñoz D, Martín-Rodríguez R, Orue I, Alonso J, García-Prieto A, et al. Magnetic study of Co-doped magnetosome chains. J Phys Chem C. 2018;122(13):7541–50.
27. Munoz D, Marcano L, Martin-Rodriguez R, Simonelli L, Serrano A, Garcia-Prieto A, et al. Magnetosomes could be protective shields against metal stress in magnetotactic bacteria. Sci Rep. 2020;10(1):11430.
28. Li W, Zeng G, Yan J, Liu X, Jiang X, Yang J, et al. One-pot green synthesis of I@CNDs-Fe3O4 hybrid nanoparticles from kelp for multi-modal imaging in vivo. Mater Sci Eng C Mater Biol Appl. 2021;124: 112037.
29. Staniland S, Williams W, Telling N, Van Der Laan G, Harrison A, Ward B. Controlled cobalt doping of magnetosomes in vivo. Nat Nanotechnol. 2008;3(3):158–62.
30. Alphandéry E, Carvallo C, Menguy N, Chebbi I. Chains of cobalt doped magnetosomes extracted from AMB-1 magnetotactic bacteria for application in alternative magnetic field cancer therapy. J Phys Chem C. 2011;115(24):11920–4.
31. Li W, Guo F, Ling H, Zhang P, Yi M, Wang L, et al. High-performance nonvolatile organic field-effect transistor memory based on organic semiconductor heterostructures of pentacene/P13/pentacene as both charge transport and trapping layers. Adv Sci (Weinh). 2017;4(8):1700007.

Xu *et al. Journal of Nanobiotechnology*   (2022) 20:364

Page 14 of 14

32. Ali I, Peng C, Khan ZM, Naz I. Yield cultivation of magnetotactic bacteria and magnetosomes: a review. J Basic Microbiol. 2017;57(8):643–52.
33. Yan X, Zhang DW, Liu C, Bao W, Wang S, Ding S, et al. High performance amplifier element realization via MoS2/GaTe heterostructures. Adv Sci (Weinh). 2018;5(4):1700830.
34. Kashyap M, Samadhiya K, Ghosh A, Anand V, Lee H, Sawamoto N, et al. Synthesis, characterization and application of intracellular Ag/AgCl nanohybrids biosynthesized in Scenedesmus sp. as neutral lipid inducer and antibacterial agent. Environ Res. 2021;201: 111499.
35. Taubes G. The bacteria fight back. Science. 2008;321:356–61.
36. Lakkim V, Reddy MC, Pallavali RR, Reddy KR, Reddy CV, Inamuddin AL, Bilgrami DL. Green synthesis of silver nanoparticles and evaluation of their antibacterial activity against multidrug-resistant bacteria and wound healing efficacy using a murine model. Antibiotics. 2020;9(12):902. https://doi.org/10.3390/antibiotics9120902.
37. Wright GD. The antibiotic resistome: the nexus of chemical and genetic diversity. Nat Rev Microbiol. 2007;5(3):175–86.
38. Yang X, Yang J, Wang L, Ran B, Jia Y, Zhang L, et al. Pharmaceutical intermediate-modified gold nanoparticles: against multidrug-resistant bacteria and wound-healing application via an electrospun scaffold. ACS Nano. 2017;11(6):5737–45.
39. Pang Q, Lou D, Li S, Wang G, Qiao B, Dong S, et al. Smart flexible electronics-integrated wound dressing for real-time monitoring and on-demand treatment of infected wounds. Adv Sci (Weinh). 2020;7(6):1902673.
40. Wang S, Zheng H, Zhou L, Cheng F, Liu Z, Zhang H, et al. Nanoenzyme-reinforced injectable hydrogel for healing diabetic wounds infected with multidrug resistant bacteria. Nano Lett. 2020;20(7):5149–58.
41. Wu J, Zhu J, Wu Q, An Y, Wang K, Xuan T, et al. Mussel-inspired surface immobilization of heparin on magnetic nanoparticles for enhanced wound repair via sustained release of a growth factor and M2 macrophage polarization. ACS Appl Mater Interfaces. 2021;13(2):2230–44.
42. Xu L, Wang YY, Huang J, Chen CY, Wang ZX, Xie H. Silver nanoparticles: synthesis, medical applications and biosafety. Theranostics. 2020;10(20):8996–9031.
43. Thangavel P, Ramachandran B, Chakraborty S, Kannan R, Lonchin S, Muthuvijayan V. Accelerated healing of diabetic wounds treated with L-glutamic acid loaded hydrogels through enhanced collagen deposition and angiogenesis: an in vivo study. Sci Rep. 2017;7(1):10701.
44. Guo F, Liu Y, Chen Y, Tang T, Jiang W, Li Y, et al. A novel rapid and continuous procedure for large-scale purification of magnetosomes from *Magnetospirillum gryphiswaldense*. Appl Microbiol Biotechnol. 2011;90(4):1277–83.
45. Honda T, Tanaka T, Yoshino T. Stoichiometrically controlled immobilization of multiple enzymes on magnetic nanoparticles by the magnetosome display system for efficient cellulose hydrolysis. Biomacromol. 2015;16(12):3863–8.
46. Zhang L, Dou YH, Gu HC. Synthesis of Ag-Fe3O4 heterodimeric nanoparticles. J Colloid Interface Sci. 2006;297(2):660–4.
47. Gu HW, Yang ZM, Gao JH, Chang CK, Xu B. Heterodimers of nanoparticles: formation at a liquid–liquid interface and particle-specific surface modification by functional molecules. J Am Chen Soc. 2005;127:34–5.
48. Zhang H, Yang Z, Ju Y, Chu X, Ding Y, Huang X, et al. Galvanic displacement synthesis of monodisperse janus- and satellite-like plasmonic-magnetic Ag-Fe@Fe3O4 heterostructures with reduced cytotoxicity. Adv Sci (Weinh). 2018;5(8):1800271.
49. Das MC, Sandhu P, Gupta P, Rudrapaul P, De UC, Tribedi P, et al. Attenuation of *Pseudomonas aeruginosa* biofilm formation by Vitexin: a combinatorial study with azithromycin and gentamicin. Sci Rep. 2016;6:23347.
50. Rishi P, Vij S, Maurya IK, Kaur UJ, Bharati S, Tewari R. Peptides as adjuvants for ampicillin and oxacillin against methicillin-resistant *Staphylococcus aureus* (MRSA). Microb Pathog. 2018;124:11–20.
51. Sader HS, Jones RN. Comprehensive in vitro evaluation of cefepime combined with aztreonam or ampicillin/sulbactam against multi-drug resistant *Pseudomonas aeruginosa* and *Acinetobacter* spp. Int J Antimicrob Agents. 2005;25(5):380–4.
52. Hassoun-Kheir N, Stabholz Y, Kreft JU, de la Cruz R, Romalde JL, Nesme J, et al. Comparison of antibiotic-resistant bacteria and antibiotic resistance genes abundance in hospital and community wastewater: a systematic review. Sci Total Environ. 2020;743: 140804.
53. Imran M, Jha SK, Hasan N, Insaf A, Shrestha J, Shrestha J, et al. Overcoming multidrug resistance of antibiotics via nanodelivery systems. Pharmaceutics. 2022. https://doi.org/10.3390/pharmaceutics14030586.
54. Yin IX, Zhang J, Zhao IS, Mei ML, Li Q, Chu CH. The antibacterial mechanism of silver nanoparticles and its application in dentistry. Int J Nanomed. 2020;15:2555–62.
55. Vila Dominguez A, AyerbeAlgaba R, Miro Canturri A, Rodriguez Villodres A, Smani Y. Antibacterial activity of colloidal silver against gram-negative and gram-positive bacteria. Antibiotics (Basel). 2020. https://doi.org/10.3390/antibiotics9010036.
56. Hadrup N, Sharma AK, Loeschner K. Toxicity of silver ions, metallic silver, and silver nanoparticle materials after in vivo dermal and mucosal surface exposure: a review. Regul Toxicol Pharmacol. 2018;98:257–67.
57. Abdulsada Z, Kibbee R, Schwertfeger D, Princz J, DeRosa M, Ormeci B. Fate and removal of silver nanoparticles during sludge conditioning and their impact on soil health after simulated land application. Water Res. 2021;206: 117757.
58. Panacek A, Kvitek L, Smekalova M, Vecerova R, Kolar M, Roderova M, et al. Bacterial resistance to silver nanoparticles and how to overcome it. Nat Nanotechnol. 2018;13(1):65–71.
59. Pieretti JC, Goncalves MC, Nakazato G, Santos de Souza AC, Boudier A, Seabra AB. Multifunctional hybrid nanoplatform based on Fe3O4@Ag NPs for nitric oxide delivery: development, characterization, therapeutic efficacy, and hemocompatibility. J Mater Sci Mater Med. 2021;32(3):23.
60. Ghaseminezhad SM, Shojaosadati SA, Meyer RL. Ag/Fe3O4 nanocomposites penetrate and eradicate *S. aureus* biofilm in an in vitro chronic wound model. Colloids Surf B Biointerfaces. 2018;163:192–200.
61. Bassetti S, Tschudin-Sutter S, Egli A, Osthoff M. Optimizing antibiotic therapies to reduce the risk of bacterial resistance. Eur J Intern Med. 2022. https://doi.org/10.1016/j.ejim.2022.01.029.
62. Mikhailova EO. Silver nanoparticles: mechanism of action and probable bio-application. J Funct Biomater. 2020. https://doi.org/10.3390/jfb11040084.
63. Wright JA, Richards T, Srai SK. The role of iron in the skin and cutaneous wound healing. Front Pharmacol. 2014;5:156.
64. Belvedere R, Pessolano E, Novizio N, Tosco A, Eletto D, Porta A, et al. The promising pro-healing role of the association of mesoglycan and lactoferrin on skin lesions. Eur J Pharm Sci. 2021;163: 105886.
65. Yu N, Cai T, Sun Y, Jiang C, Xiong H, Li Y, et al. A novel antibacterial agent based on AgNPs and Fe3O4 loaded chitin microspheres with peroxidase-like activity for synergistic antibacterial activity and wound-healing. Int J Pharm. 2018;552(1–2):277–87.
66. Friedrich RP, Cicha I, Alexiou C. Iron oxide nanoparticles in regenerative medicine and tissue engineering. Nanomaterials (Basel). 2021. https://doi.org/10.3390/nano11092337.
67. Vargas G, Cypriano J, Correa T, Leao P, Bazylinski DA, Abreu F. Applications of magnetotactic bacteria, magnetosomes and magnetosome crystals in biotechnology and nanotechnology: mini-review. Molecules. 2018. https://doi.org/10.3390/molecules23102438.
68. Mathuriya AS. Magnetotactic bacteria: nanodrivers of the future. Crit Rev Biotechnol. 2015;36(5):788–802.
69. Sanchez LM, Alvarez VA. Advances in magnetic noble metal/iron-based oxide hybrid nanoparticles as biomedical devices. Bioengineering (Basel). 2019. https://doi.org/10.3390/bioengineering6030075.
70. Amor M, Ceballos A, Wan J, Simon CP, Aron AT, Chang CJ, et al. Magnetotactic bacteria accumulate a large pool of iron distinct from their magnetite crystals. Appl Environ Microbiol. 2020. https://doi.org/10.1128/AEM.01278-20.
71. Zhang Y, Zhang X, Jiang W, Li Y, Li J. Semicontinuous culture of Magnetospirillum gryphiswaldense MSR-1 cells in an autofermentor by nutrient-balanced and isosmotic feeding strategies. Appl Environ Microbiol. 2011;77(17):5851–6.
72. Suppi S, Kasemets K, Ivask A, Kunnis-Beres K, Sihtmae M, Kurvet I, et al. A novel method for comparison of biocidal properties of nanomaterials to bacteria, yeasts and algae. J Hazard Mater. 2015;286:75–84.

Publisher's Note

Springer Nature remains neutral with regard to jurisdictional claims in published maps and institutional affiliations.